

**DESIGN OF FRP STRENGTHED METALIC
HEMISPHERE DOMES SUBJECTED TO EXTERNAL
PRESSURE**

Industrial project report submitted in partial fulfilment of
the requirements for the award of the degree.

B. TECH (MECHANICAL ENGINEERING)

BY

G VENKATA MARUTHI ABHIRAM (208W1A03C9)

Under the supervision of

T. GOPI KRISHNA

SCIENTIST E, DRDL

And

Dr. M. BALAJI,

ASSOCIATE PROFESSOR, VRSEC



Missiles And Strategic Systems (MSS)

**Defense Research and Development
Organization**

Kanchanbagh, Hyderabad –500058

DEPARTMENT OF MECHANICAL ENGINEERING

V.R. SIDDHARTHA ENGINEERING COLLEGE



CERTIFICATE

This is to certify that the thesis entitled "**DESIGN OF FRP STRENGTHED METALIC HEMISPHERE DOMES SUBJECTED TO EXTERNAL PRESSURE**" submitted by **G VENKATA MARUTHI ABHIRAM (208W1A03C9)** to V. R. Siddhartha Engineering College, Vijayawada under the jurisdiction of JNTU Kakinada in partial fulfillment of the requirements for the award of the degree of **Bachelors of Technology** is a record of Bonafide research work carried out by us under our supervision and guidance. This work has not been submitted elsewhere for the award of any degree.

T. GOPI KRISHNA

SCIENTIST E, DRDL

Dr. N. VIJAYASAI

HEAD OF DEPT, VRSEC

Dr. M. BALAJI

ASSOCIATE PROFFESSOR, VRSEC

ACKNOWLEDGEMENT

We would like to extend our heartfelt thanks to our project guide **Dr.T.Gopi Krishna, Scientist E (DRDL) and Dr. M. Balaji, Associate Professor**, VRSEC whose guidance and support have been invaluable throughout the completion of this project. Their expertise and insightful suggestions have shaped the project's direction and inspired us to achieve our goals.

Furthermore, we would like to express our gratitude to all the technical officers and technicians involved in this project. Their dedication, expertise, and prompt support have been crucial in overcoming technical challenges and ensuring smooth project execution.

We wish to extend our sincere thanks to **Dr. N. VIJAYA SAI, Professor and Head of the Mechanical Engineering Department**, for his encouragement.

TABLE OF CONTENTS

Section No	Description	Page No
Chapter-1	Introduction	1
1.1	Introduction	1-2
1.2	Background and motivation	2-4
1.3	Buckling behavior	4-6
1.4	Objectives and Advantages	6-9
Chapter-2	Literature Review	10-14
Chapter-3	Modelling the buckling characteristics of metal – FRP hybrid shells	15-16
Chapter-4	Effectiveness of FRP strength on buckling behavior of metal FRP hybrid shells.	17-18
4.1	Development Of Different Cases Of Hemispherical Hybrid Shells.	18-23
4.2	Modeling for FEA with boundary conditions and geometric imperfections	23-27
4.3	Experiment Validation	27-28
4.4	Effect of FRP Strengthening on buckling behavior	29-32
4.5	Final Buckling Performance	32-38
Chapter-5	Live Testing And Examination	39-43
Chapter-6	Summary, Conclusion and Future Scope	15-15

ABSTRACT

Thin metallic cylindrical shell structures wrapped externally with one or multiple layers of fiber-reinforced polymer (FRP) composite sheets exhibit a significant increase in buckling capacity and ductility. The existing research is minimal, limited to shells of specific radius-to-thickness ratios, and often reported only the buckling capacity and ductility percentage increase. This research is intended to bridge this gap and provide a comprehensive understanding of the buckling behavior of metal-FRP hybrid shell structures. It focusses on 1) detailed numerical modeling addressing different aspects as well as non-linearities viz. intra-laminar and interfacial damage specific to metal-FRP hybrid shells, 2) effectiveness of FRP strengthening and effective FRP strengthening methods for metallic shells of all possible ratios, 3) imperfection sensitivity of hybrid shells of different ratios, 4) the effect of cut-outs in thin airframe hybrid shells of higher ratios, and 5) experimental validation of buckling characteristics of both the metallic and metal-FRP hybrid airframe plain cylindrical shells. Thus, the thesis brings out the following aspects of metal-FRP hybrid shells: 1) the effect of interfacial and intraluminal FRP damage on buckling behavior, 2) the effectiveness of FRP strengthening on the general buckling behavior of shells of different ratios, 3) the sensitivity to imperfections, 4) the effect of unstiffened and stiffened cut-outs on elastically buckling shells, and 5) the methods to assess bond quality, measurement of imperfections and experimental validation.

Key Words: Metal-FRP, Buckling Characteristics, Bond Quality, Buckling Behaviour.

FIGURES

Sl.No	Fig No	Caption	Page No
1	1.1	The difference in buckling behavior of different structural members .	4
2	2.1	Linear Analysis	13
3	2.2	Non Linear	13
4	4.3	FEA simulations and experimental results	23
5	4.4	Different stages of buckling	24
6	4.5	buckling analysis with 3mm thickness of steel.	28
7	4.6	Buckling analysis with 2.5mm thickness of steel and composite mix with carbon epoxy.	29
8	4.7	Meshing of steel	30
9	4.8	Meshing of carbon epoxy	30
10	4.9	Combined mesh	31
11	4.10	The buckling analysis with 2mm composite thickness and 1mm steel.	31
12	4.11	analysis done with 1.5mm steel and 1.5 mm thickness of composite	32
13	5.1	Hemisphere with carbon epoxy on one side and steel on the other side.	33
14	5.2	Buckle testing apparatus for cylinders.	34
15	5.3	Buckle testing apparatus for hemisphere and (b), (c) shows after buckling.	36

TABLES

Sl. No	Table No	Caption	Page No
1	4.1	Geometric details of aluminum shell types employed in the numerical study	15
2	4.2	Isotropic material properties of AA2014 employed for shell	15
3	4.3	Elastic buckling and yield capacities of different shell types employed in the study	16
4	4.4	General material properties of FRP wrap	20
5	4.5	Shell types and cases of FRP strengthening studied	20
6	4.6	Shell types and cases of FRP strengthening studied	21
7	4.7	The results table of variety of thicknesses and their corresponding load factors.	32

NOMENCLATURE

Symbol	Caption
FRP	Fiber Reinforced Polymer
as	Anti-Symmetry
s	Symmetry

Chapter-1

INTRODUCTION

1.1 Introduction:

Fiber Reinforced Polymer (FRP) composites have become integral components in various industries, including civil infrastructure, automotive, aerospace, wind energy, sports, and marine applications. Their prevalence in load-bearing structures highlights the need for robust joining methods, given that mechanical processes like bolting or riveting can introduce stress concentrations and weak spots in the structure. The adverse effects of stress concentrations are particularly pronounced at the contact points between fasteners and hole-surfaces, necessitating careful design considerations.

In FRP composite structures, the conventional mechanical joining methods are further challenged by stress concentrations and singularities arising from fiber discontinuities caused by the fabrication process. To address these challenges, adhesive bonding processes emerge as a preferred alternative, offering high strength, stiffness, and fatigue life. This becomes especially crucial in the aerospace and civil infrastructural domains, where flat or curved panels with adhesively bonded frames and stiffeners are frequently employed.

The trend towards miniaturization and enhanced performance in modern microelectronic packages introduces multilayered structures, subjected to thermal excursions during fabrication and assembly. The resulting thermo-mechanical stresses, stemming from the mismatch in coefficients of thermal expansion among different material layers, can lead to interfacial delamination—a significant concern in microelectronic package failure. Adhesive bonding stands out as a solution, providing not only strength and stiffness but also automation feasibility in contrast to traditional joining methods.

The choice of Graphite/Epoxy composite materials, particularly in space applications, is motivated by their exceptional strength-to-weight ratio and near-zero coefficient of thermal expansion. As the use of composite materials continues to

replace conventional ones, the significance of adhesive bonding in joining composite laminated panels cannot be overstated.

However, challenges persist in identifying and studying damage initiation and propagation in adhesive bonded joints, whether in structural applications or microelectronic packages. Manufacturing defects and excessive loading can lead to damage, emphasizing the need for a thorough understanding of the behavior of these joints under specific conditions.

In the realm of microelectronic packages, interfacial delamination is a prevalent failure mode, driven by the mismatch in coefficients of thermal expansion. Experimental methods such as tab pull tests and button shear tests have been employed, but their quantitative results often present challenges. This has led to a preference for a fracture mechanics approach over stress-based analyses, particularly in the face of complex geometries and varying material properties.

1.2 Background and Motivation

FRP strengthening of metallic structures is a relatively new topic that has witnessed interest in varied fields of application. Strengthening of metallic structures by adhesive bonding of fiber-reinforced polymer (FRP) sheets has been successfully employed for 1) the repair of damaged metallic airframe components to restore their original design strength by employing bonded composite patches or reinforcements (Baker et al. [2], Srilakshmi et al. [3], Matta et al. [4]); 2) flexural strengthening of metallic beams by adhesive bonding of FRP laminates on the soffit side of beams (Schnurch and Rizkalla [5], Tavakkolizadeh and Saadatmanesh [6], Narayananamurthy et al. [7]); 3) enhancing the stability of slender metallic structural components subjected inelastic local buckling near joints (El-Tawil and Ekiz [8], Shaat and Fam [9], Harries et al. [10], Bambach and Elchalakani [11], Bambach et al. [12], Kumar and Senthil [13], Madhavan et al. [14]); and 4) strengthening of thin-walled metallic sections subjected to shell buckling modes (Haedir and Zhao [15], Teng and Hu [16]). Thin-walled shell structures subjected to axial compressive loads have broad applications in aerospace vehicles, silos, and tanks for bulk solids and liquids storage, nuclear reactors, cooling towers, pressure vessels, and pipelines. These shell

structures transmit applied forces by compressive, tensile, and shear stresses in the surface plane, i.e., membrane stresses. Buckling due to axial compressive loads is the predominant failure mode, especially for bottom sections of the aerospace vehicle due to the weight of the upper stages or propulsive loads during launch. These shell structures are employed as interstage skirts and payload adapters and are designed to meet the requirements of very high load carrying capacities at a comparatively low structural weight. These shell structures have a large radius-to-thickness (r/t) ratio. Euler buckling strength for these structures is very high since the material is placed far from the axis. Shell buckling modes, a local form of buckling, control the load capacity of these thin-walled cylindrical or conical structures (Teng and Rotter [17]). The FRP strengthening of aerospace shell structures is a promising, easy-to-employ retrofit strengthening technique to enhance their buckling capacity significantly. It is also an excellent method to realize lightweight structures meeting all the structural and dimensional accuracy requirements, with added advantages of fast realization time and minimum infrastructure. These hybrid structures will also have added benefit of higher vibration attenuation compared to their metallic counterparts.

Vibration attenuation is vital in restricting the vibration levels of the shell-mounted onboard electrical and electronic packages within their qualification limits. In the last couple of decades, significant research has been carried out on pure metallic (Arbocz and Starnes [18]) and composite (Hilburger et al. [19], Bisagni [20]) shell structures subjected to axial buckling. There are even well-established standards for the design of these structures against buckling (EN 1993-1-6: Eurocode 3 [21]). On the other hand, the depth and breadth of research on FRP strengthened metallic shell structures subjected to axial buckling is limited. There exist many research gaps, and there is a lack of holistic understanding of the axial buckling behavior of these metal FRP hybrid shell structures. Therefore, this thesis is devoted to bringing out clarity and a better understanding of the buckling behavior of FRP strengthened metallic cylindrical shell structures.

- To identify the location of damage initiation in Sliding, Scissoring and opening modes.
- Crack propagation envelops at different strains

1.3 Buckling Behavior

The extent of strengthening achievable with FRP for metallic cylindrical shells depends on the metallic shell structures' inherent buckling characteristics, which are fundamentally different from other structural members, viz. columns and plates as brought out by Pircher and Bridge [22] in Figure 1.1.

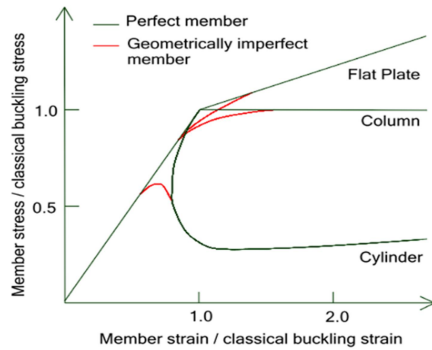


Figure 1.1: The difference in buckling behavior of different structural members .

All three structural members show a linear response until the critical load is attained. The response post-buckling is undefined for perfect columns due to their inability to develop transverse stresses to restrain out-of-plane displacements. Imperfection in a geometrically imperfect column increases lateral displacements resulting in the attainment of maximum load asymptotically. Since the plate can generate transverse tensile stresses to work against the growth of out-of-plane displacements, the load capacity of flat plates increases even after the critical load is attained. A geometrically imperfect plate approaches the load capacity of a perfect plate asymptotically, with a smoothed kink as shown in Fig. 1.1. However, the post-buckling response of an elastically buckling perfect shell is markedly different. A steep fall in axial load would ensue after the critical load was attained. The linear pre-buckling path ends abruptly with the instantaneous appearance of asymmetric buckling modes spread around the circumference and along several rows longitudinally, resulting in shell bifurcation. At the point of buckling, hundreds of buckling modes would become simultaneously critical. Fast switching over from one mode to the other happens after bifurcation, resulting in an unstable post-buckling path. Imperfections in shell structures can drastically reduce the buckling load, as the

narrow gap between re- and post-buckling segments of the buckling curve is bridged at much lower levels, as shown in Figure 1.1. A detailed investigation of axial compression in cylindrical shells is given by Teng and Rotter [17]. Cylindrical shells are equipped with a relatively high $\text{Euler Buckling Stress} / \text{Axial Load}$ ratio. Euler buckling stress for these kinds of shell structures is very high since all the material is placed far from the axis, making these structures the most efficient form for withstanding compressive loads. Shell buckling modes, which are the local forms of buckling, are the failure mode of these structures, in which large deformations in the shell surface perpendicular to the loading direction occur.

1.4 Objectives:

Aerospace: Single lap joints are widely used in aircraft manufacturing for bonding structural components such as wings, fuselage panels, and tail sections. The lightweight nature of adhesive bonding helps reduce overall aircraft weight, leading to improved fuel efficiency and performance.

Automotive: In the automotive industry, single lap joints are utilized for bonding components in vehicle bodies, such as roof panels, door panels, and chassis components. Adhesive bonding provides high strength and stiffness, contributing to improved vehicle safety and structural integrity.

Marine: Adhesively bonded single lap joints are employed in boat and shipbuilding for joining hull panels, decks, bulkheads, and other structural components. The use of adhesive bonding helps reduce weight, minimize corrosion, and enhance overall structural integrity in marine environments.

Wind Energy: Single lap joints are essential in the construction of wind turbine blades, where they are used to bond composite materials together. Adhesive bonding provides high strength and durability, allowing the blades to withstand the harsh operating conditions encountered in wind energy applications.

Construction: In the construction industry, single lap joints are utilized for bonding structural components in buildings and infrastructure projects. They are commonly used for joining prefabricated panels, facades, and other architectural elements, providing a strong and reliable connection.

Electronics: Adhesively bonded single lap joints are employed in the assembly of electronic devices and components. They are used for bonding circuit boards, display panels, and other electronic components, providing a lightweight and reliable connection while minimizing the risk of damage to sensitive electronic components.

Medical: Single lap joints find applications in the medical field for bonding biomedical devices and implants. Adhesive bonding techniques are used to join materials such as metals, ceramics, and polymers, providing biocompatible and sterile connections for medical devices and implants.

Advantages:

High Strength-to-Weight Ratio: FRP materials, such as carbon fiber or fiberglass, have a high strength-to-weight ratio, making them lightweight yet strong. When used in adhesively bonded joints, they contribute to overall weight reduction while maintaining structural integrity, particularly beneficial in aerospace, automotive, and marine applications.

Corrosion Resistance: FRP materials are inherently resistant to corrosion, unlike metals such as steel or aluminum. Adhesively bonding FRP joints eliminates the need for metal fasteners, reducing the risk of galvanic corrosion and improving durability, especially in harsh environments like marine or chemical processing facilities.

Tailored Mechanical Properties: FRP materials can be engineered to have specific mechanical properties, such as stiffness, strength, and fatigue resistance, through variations in fiber orientation, resin type, and manufacturing processes. Adhesively bonded joints allow for the precise alignment of fibers and the optimization of load transfer, resulting in joints that are tailored to meet the requirements of specific applications.

Fatigue Resistance: FRP materials exhibit excellent fatigue resistance, particularly when compared to metals. Adhesively bonded joints with FRP materials distribute stress more evenly across the joint, reducing the risk of fatigue failure and extending the service life of structures subjected to cyclic loading, such as bridges, wind turbine blades, and aerospace components.

Design Flexibility: FRP materials offer greater design flexibility compared to traditional materials like steel or concrete. They can be molded into complex shapes

and configurations, allowing for innovative joint designs that optimize structural performance and minimize material usage.

Electrical Insulation: FRP materials are electrically non-conductive, making them suitable for applications where electrical insulation is required. Adhesively bonded FRP joints provide a seamless connection that maintains the electrical insulation properties of the material, useful in industries such as electronics and telecommunications.

Environmental Resistance: FRP materials are resistant to a wide range of environmental conditions, including UV radiation, moisture, and temperature fluctuations. Adhesively bonded joints with FRP materials provide a weatherproof seal that protects the underlying substrate from degradation, extending the lifespan of structures exposed to outdoor environments.

Ease of Installation: Adhesively bonded joints with FRP materials are often easier and quicker to install compared to traditional joints requiring welding, bolting, or riveting.

Chapter-2

Literature Review

W. QIAN and C.T. SUN [1] Methods for calculating stress intensity factors for interfacial cracks between two orthotropic solids. The finite element methods in conjunction with crack closure technique were used to calculate these finite extension strain energy release rates from which accurate stress intensity factors were obtained.

Nilima Roy, Arpan Das, Ashok Kumar Ray [2] In this paper creep damage assessment of 12 years' service exposed HP-40 grade of steel used in hydrogen reformer of a petrochemical industry has been carried out in terms of a discontinuous Markov process. Experimentally determined conventional creep data under identical testing condition were used in the present investigation.

R. Ganesan [3] Fatigue damage accumulation in engineering materials is usually quantified using a suitable damage parameter that can serve as a reliable descriptor of damage development. Tests are conducted on material samples in order to collect sample data about damage development.

N. Roy, S.C. Bose, R.N. Ghosh [4] a stochastic model for the creep damage evolution and associated scatter in austenitic stainless steel has been developed in terms of a discontinuous Markov process. The magnitude of damage has been described in the form of a probability distribution function whose evolution in time characterizes the non-deterministic nature of the damage accumulation process.

N.P. O'Dowd, C.F. Shih and M.G. Stout [5] Test geometries for measuring interfacial fracture toughness. The mechanical integrity of many electronic devices and their components is determined by the strength of the interfaces between dissimilar materials.

Viswanathan Sundararaman and Barry D. Davidson [6] An unsymmetric double cantilever beam test for interfacial fracture toughness determination. Due to the dissimilar in-plane and out-of-plane deformations of the two legs, the load vs deflection response of the specimen is found to be nonlinear.

Hongqin Yang [7] a three-term interaction crack growth model developed

for creep-brittle materials is restudied. Derivation of cycle-time interaction intensity factor from the Gaussian equation is discussed. Crack growth behaviour of a nickel-based powder metallurgy super alloy has been studied under elevated temperatures.

J.R. Rice [8] A path independent integral and the approximate analysis of strain concentration by notches and cracks. Contained perfectly plastic deformation near a crack tip is analyzed for the plane-strain case with the aid of the slip-line theory.

E.F. Rybicki et al. [9] an efficient technique for evaluating stress intensity factors is presented. The method, based on the crack closure integral, can be used with a constant strain finite element stress analysis and a coarse grid. The technique also permits evaluation of both Mode I and Mode II stress intensity factors from the results of a single analysis. Example computations are performed for a double cantilever beam test specimen, a finite width strip with a central crack, and a pin loaded circular hole with radial cracks.

Lanqing Tang, Caifu Qian [10] Experimental studies on I + II mixed mode notch-crack fatigue propagation in austenitic stainless steel 06Cr19Ni10 were carried out with consideration of the strain-strengthening effects. It is found that after initiating from the notch-crack tip, the new crack changes from I + II mixed mode to Mode I. Strain-strengthening has no effects on the crack growth path, but has some effects on the crack growth rates.

Carla Beckmann [11] The present study is concerned with a numerical analysis of the uncertainties in the response of foam core sandwich structures caused by the uncertain microstructure of the core material.

Jialai Wang [12] Developed cohesive zone models to simulate the initiation and growth of intermediate crack induced de-bonding, and interfacial crack de-bonding, under mixed mode loading. Jialai Wang observed that from the point of view of cohesive zone model, expression relating two parameters, and fracture energy and slips between FRP plate and concrete, are sufficient in determining the initiation and growth load of intermediate crack de-bonding.

Laura De Lorenzis and Giorgio Zavarise [13] Analytically studied the interface behavior of the integrated structure made of quasi-brittle rigid substrate

and FRP sheet adherends under mixed-mode loading using LEFM energy approach and cohesive zone model approach in the peel test configuration. Laura De Lorenzis and Giorgio Zavarise observed that the interface which is typically influenced by the distribution of the interfacial shear stresses.

Yuval Freed and Leslie Banks-Sills [14] Proposed new two-dimensional cohesive zone model to predict mixed mode interface fracture in bi-materials based on analytical and experimental observations. Yuval Freed and Leslie Banks-Sills described the cohesive model as an infinite set of cohesive laws, one for each discrete value of the phase angle. For each model, two parameters, the cohesive energy and cohesive strength will specify the cohesive law for the current phase angle.

Balzani and Wagner [15] used cohesive zone approach to describe three-dimensional mixed mode delamination, by using FE which calculates only inter-laminar stresses from the standard solid element formulations. Balzani and Wagner observed that numerical solutions of the exponential model had superior convergence behavior than from linear softening model.

Naghdi Choupani [16] used plane strain FEA to study Cohesive, interfacial, and inter-laminar fracture behavior of cracks in Lap Joints with isotropic adherends. Naghdi Choupani used fracture mechanics-based approach for the determination of SIF and SERRs from J integral and stress-based approach to predict the failure of adhesively bonded DLJs. Naghdi Choupani observed that as the crack length increases both shearing and opening mode stress intensity factors increase, but their amplitudes are not responsive to adhesive thickness.

K. Kimura, H. Kushima, F. Abe, K. Yagi [17] Inherent creep strength is defined as a constant creep strength independent of time and microstructure. Sigmoidal inflection of a relation between stress and time to rupture is explainable in terms of a loss of creep strength followed by the advent of inherent creep strength.

S.K. Jeswal [18] in this article, a novel approach for solving static structural problems based on Artificial Neural Network (ANN) has been presented. Various numerical methods are available to solve static problems of structures having crisp parameters by converting the problem to algebraic

systems.

R. Venkata Kiran Kumar [19] et al. made fracture analysis on adhesive bonded[+θ/-θ]s FRP laminated composite Single Lap Joint (SLJ) is carried out by varying fiber angle (θ) to predict location of initiation of damage propagation by evaluating fracture parameter Energy Release Rate(G) using VCCT technique.

R. Venkata Kiran Kumar et al [20]. made predictions on distribution of Strain Energy Release Rates (SERR) along the delamination front using fracture mechanics based Virtual Crack Closure Technique (VCCT).

Chapter-3

Methodology

3.1 Modelling the buckling characteristics of metal – FRP hybrid shells

This chapter presents the development of a comprehensive numerical model for carrying out the buckling analysis of metal-FRP hybrid structures. Different aspects specific to metal-FRP shell structures, viz. modeling FRP overlap, locating shell element's reference surface, and distribution of integration points across the thickness of shell surface, are taken into account. Also, all the non-linearities involved in modeling metal-FRP hybrid shells, viz. surface imperfections, metal-FRP interfacial bond behavior, and intralaminar FRP damage, are addressed. The effect of metal-FRP interfacial bond damage and intra-laminar FRP damage on buckling behavior of metal FRP hybrid shells is brought out in the second part of this chapter. Experimental work of Teng and Hu [16] on plastically buckling metal-FRP hybrid steel shells, strengthened with multiple layers of glass FRP (GFRP) sheets, was used as a reference for validating the numerical model. A better insight into the buckling behavior of these hybrid shell structures is delineated.

The geometry of the cylindrical shell investigated in the present study was adopted from specimens from experiments by Teng and Hu [16], as shown in Figure 2.1(a). The diameter of hemisphere shell is 800mm and a thickness of 10mm.

Fast switching over from one mode to the other happens after bifurcation, resulting in an unstable post-buckling path. Imperfections in shell structures can drastically reduce the buckling load, as the narrow gap between re- and post-buckling segments of the buckling curve is bridged at much lower levels, as shown in Figure 1.1. All three structural members show a linear response until the critical load is attained. The response post-buckling is undefined for perfect columns due to their inability to develop transverse stresses to restrain out-of-plane displacements. Imperfection in a geometrically imperfect column increases lateral displacements resulting in the attainment of maximum load asymptotically

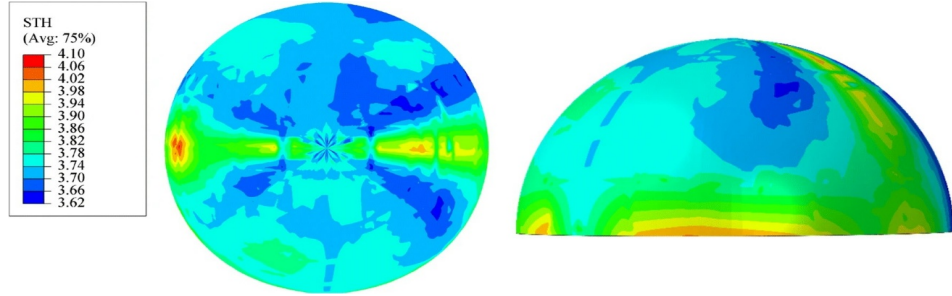


Figure 2.1

The buckling analysis of the hemisphere is done by using the software ABAQUS and there are many factors which effects the buckling of a material. In fig 2.2 we can clearly see the various buckling analysis done the hemisphere.

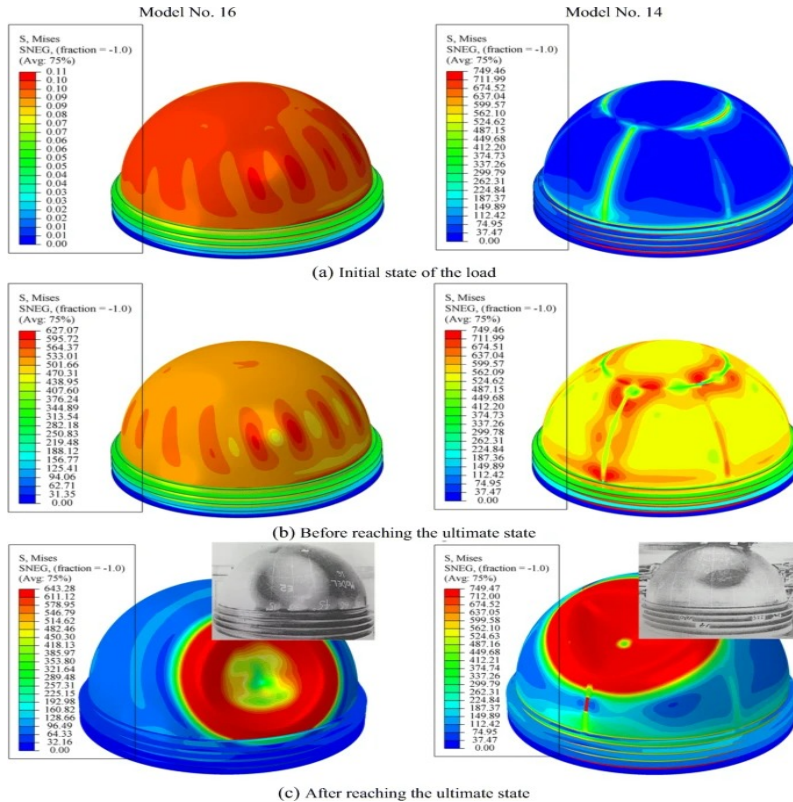


Figure 2.2

Chapter-4

Effectiveness of FRP strengthening on buckling behavior of metal-FRP hybrid shells.

The studies presented in the previous chapter provided a prospect of enhancement in structural buckling performance of metallic cylindrical shells after external wrapping with one or more layers of fiber-reinforced polymer (FRP) composite. The enhancement in buckling characteristics of the original metallic shell was evidenced by the increase in buckling load capacity, ductility, or a combination of both. The versatility of FRP strengthening comes from the ease of strengthening and the possibility of meeting a variety of different combinations of strengthening requirements. This was achieved due to the directional properties of FRP materials and the availability of FRP sheets with a vast range of modulus and strength. However, strengthening against shell buckling was a challenge because of the proximity of the number of buckling modes and the number of different ways a metallic shell structure can buckle [74]. Strengthening design depends on the buckling failure modes of bare metallic shells. Depending on the modulus, radius, thickness, and strength of the metallic shell, the shell would be subjected to either elastic or plastic buckling.

This work numerically studied the FRP strengthening of shells undergoing all possible shell buckling modes and buckling characteristics. The changes in buckling modes and buckling characteristics of a bare aluminum shell with changes in ratio; the effectiveness of FRP strengthening on shells undergoing different varieties of buckling phenomena; different stages in the buckling behavior of FRP strengthened shells; and the changes in buckling behavior with the direction and amount of FRP strengthening were investigated. The complete numerical results are summarized, and the increase in axial capacity and the change in ductility with the direction and amount of FRP strengthening is graphically presented. Recommendations are proposed on the appropriate type of FRP strengthening and limits of strengthening for shells exhibiting different types of buckling behavior.

4.1 DEVELOPMENT OF DIFFERENT CASES OF HEMISPHERICAL HYBRID SHELLS.

The design of FRP strengthening to achieve the required increase in axial load capacity and ductility of cylindrical shells requires a good understanding of buckling characteristics and modes of the bare metallic shell. To cover the shells undergoing all possible varieties of buckling modes and to understand the effect of FRP strengthening, aluminum shell types named A1 to A5 with different ratios, as tabulated in Table 4.1, are considered in this study.

Shell nomenclature	Description	Shell diameter, d (mm)	Thickness, t (mm)	$\frac{r}{t}$	Length (mm)
A1	Elastic buckling	300	1	150	300
A2	Plastic buckling	300	2	75	300
A3	Plastic buckling	300	3	50	300
Special cases					
A4	Elastic buckling	300	0.3	500	300
A5	Plastic buckling	300	7.5	20	300

Table 4.1 : Geometric details of aluminum shell types employed in the numerical study

Mechanical properties of precipitation-hardened AA2014 material in T652 tempering conditions, as given in Table 4.2, were employed for the metallic shell. The mean diameter 10 and length 1024 of all the shells were maintained constant at 300 mm, and by varying the thickness of the shells, shells of different ratios were obtained.

Material property	Value
Young's modulus, E (GPa)	71
Poisson's ratio, ν	0.33
Yield strength, σ_y (MPa)	380
Tangent modulus, E_t (MPa)	780

Table 4.2: Isotropic material properties of AA2014 employed for shell [10]

Medium-length cylinders [74]. They were defined as being ‘so long’ that the end boundary conditions do not play a substantial role and ‘so short’ that the

buckling load was far below the Euler buckling load as a column. The shells with $L/\lambda > 2$ were termed as medium length cylinders in which the buckling behavior was independent of the length of the shell and boundary conditions, where λ represents the linear half wavelength of Configuration of all the shells was chosen to come under the category of meridional bending.

It can be noticed that the L/λ values of the five shells chosen for the present study are more significant than 2, as tabulated in Table 4.3. The shells are classified based on the values of elastic buckling load limit and yield capacity.

The elastic buckling load capacity was obtained by multiplying this critical elastic buckling stress by the cross-sectional area of the shell. The yield capacity of the shell was obtained by multiplying the yield strength of the material with the cross-sectional area of the shell. The buckling behavior of different types of shells with and without FRP strengthening, employed in this study, is explained here. The elastic buckling load capacity for A1-A5 shell types is tabulated in Table 4.3.

Shell nomenclatur	$\frac{r}{t}$	L/λ	σ_{cl} (MPa)	Elastic buckling load capacity (kN)	Yield capacity of the shell (kN)
A1	150	10	289	273	358
A2	75	7.1	579	1091	716
A3	50	5.8	868	2456	1074
A4	500	18.3	87	25	107
A5	20	3.7	2171	15347	2686

Table 4.3: Elastic buckling and yield capacities of different shell types employed in the study

The A1 represents the shell configuration with an ratio of 150, for which the elastic buckling load is lower than the yield load of the shell. So A1 is an elastically buckling shell. Elastic buckling means the shell buckles before the yield limit of the metallic shell is attained. Also, its configuration was so chosen that its buckling characteristics remain elastic irrespective of the direction and amount of FRP strengthening employed in this study. The A2 represents the shell configuration with an r/t ratio of 75, for which the yield load of the shell was marginally lower than the elastic buckling load. So, A2 is a plastically buckling shell. However, its configuration was so chosen that its buckling characteristics can remain plastic or change to elastic buckling depending on the direction and amount of FRP

strengthening. The A3 represents the shell configuration with an l/t ratio of 50, for which the yield capacity of the shell is relatively much lower than the elastic buckling load capacity compared to the A2 shell type. Its buckling characteristics will remain plastic for all the strengthening cases, i.e., variations in the direction and amount of FRP strengthening employed in this study. Both A2 and A3 shell types represent the plastically buckling shells undergoing asymmetrical modes of buckling post yielding. Two additional special shell types viz. A4 and A5 have been studied, representing extreme shells, buckling elastically and plastically, respectively. Case A4 represents a shell with an r/t ratio of 500. It is a very thin-walled shell with a shell thickness of 0.3 mm. Though it is still an elastically buckling shell similar to the A1 shell type, whose buckling characteristics remain elastic despite the amount and direction of FRP strengthening, it represents an extreme case of FRP strengthening. Since the FRP sheets are available with around 0.2 mm thickness, comparable with the metallic shell wall thickness, the FRP strengthening would lead to a significant amount of additional stiffening. The buckling characteristics of FRP wrap can dominate the buckling behavior of shell structure, thereby significantly altering its buckling characteristics. Case A5 represents a shell structure with an ratio of 20. It has a relatively high shell thickness compared to its diameter. It represents a special case of plastic buckling in which the bare shell buckles axisymmetrically post yielding. It is brought out in this study that the buckling characteristics of cases of FRP strengthening of other plastically buckling shells, i.e., A2 and A3 shell types, are subsets of the A5 shell type. With FRP wrapping, the strengthening of the metallic shell structure can be varied either by increasing the modulus of the FRP wrap or by increasing the number of layers of wrap of a particular modulus. So the flexural/axial stiffening of the shell wall happens for two reasons: 1) increase in effective modulus of the shell, and 2) increase in the cross-sectional area or the area moment of inertia of the shell structure. To bring out the effects of variations in FRP strengthening on buckling characteristics of the shell structure in a clear and comprehensible manner, the thickness of the FRP wrap is maintained constant at 0.17 mm, and only the modulus of the FRP wrap is varied. To investigate the cases of FRP strengthening with multiple FRP wraps, the wrap modulus was increased to large values, close to 1000 GPa. These instances of FRP strengthening with high modulus FRP wrap were equivalent representatives of FRP strengthening of the shell with multiple FRP wrap layers. By retaining the wrap thickness at 0.17 mm for all

the instances of strengthening, the cross-sectional area, and the area moment of inertia of wrap will remain the same. This procedure ensures that the axial and flexural stiffening offered by FRP wrap varies only with the modulus of the wrap. Two fundamental directions of FRP strengthening were studied here, viz. strengthening along 1) longitudinal and 2) circumferential directions, which were achieved by orienting the single layer of uni-directional FRP wrap in the direction being strengthened. For each case of strengthening studied, different instances of strengthening were generated by varying the modulus of wrap in a given direction, i.e., longitudinal or circumferential direction. For a specific case of strengthening, while varying the modulus of wrap along the circumferential or longitudinal direction, the modulus of the FRP wrap along the perpendicular direction was adjusted to maintain the effective modulus of the strengthened shell constant along the perpendicular direction. The effective modulus of the strengthened shell along direction perpendicular direction was held constant at 71 GPa, equal to the isotropic modulus of the aluminum metallic shell material. This attempt helps bring out a qualitative and clear understanding of the effects of FRP strengthening on the buckling behavior of shell structures undergoing shell buckling modes. The general properties of the uni directional FRP wrap, which were maintained constant for all the instances of strengthening, are given in Table 3.4. The different cases of FRP strengthening studied for each shell type with their nomenclatures, modulus of FRP wrap, and an effective modulus of the strengthened shell along the circumferential and longitudinal directions are provided in Table 3.5. A single-layer of FRP wrap of 0.17 mm thickness was employed in all FRP strengthened shells except for Case- 4A' and Case - 4B' for which 0.05 mm wrap thickness was employed. It can be observed from Table 3.5 that for each shell type, the effect of varying the amount (i.e., modulus) of longitudinal and circumferential directional FRP strengthening was explored. The cases of FRP strengthening for which the longitudinal modulus was varied while maintaining a constant value (i.e., at 71 GPa) for the effective circumferential modulus $\square h \square$ of the strengthened shell are named Case-#A. 60 Similarly, all the cases of FRP strengthening for which the circumferential modulus $\square h$ was varied while maintaining a constant value (i.e., at 71 GPa) for the effective longitudinal of the strengthened shell are named Case-#B, where # represents the type of shell. For example, Case-4B represents cases of FRP strengthened A4 shells, in which $\square h$ was varied while maintaining a constant value (i.e., at 71 GPa) for the

of the strengthened shell. The effective modulus of the FRP strengthened metallic shell along the longitudinal and transverse directions were calculated from the concepts of classic lamination theory) where direction 1 is defined along the longitudinal direction, 2 is defined along transverse/circumferential direction, h is the total thickness of the strengthened shell, and A11 and A22 are terms in the extensional stiffness matrix, which relates in-plane forces with corresponding strains.

4.2 Modeling for FEA with boundary conditions and geometric imperfections

The FE modeling and analysis were carried out in ABAQUS [61]. The FE model similar to Krishna et al. [77] was also employed in this study, briefly described here. The metallic cylindrical shell and the FRP wrap were modeled as two separate shell surfaces of the same diameter viz. \square 300 mm. The tie constraint was introduced between the metallic shell's outer surface and the FRP wrap's inner surface. Both the surfaces were discretized with quadrilateral shell elements (S4R), which linearly interpolate the field variable and capture the finite-membrane strain with reduced integration. These elements were more robust without leading to convergence difficulties, even in the presence of steep deformation gradients around the axisymmetric bulge region and asymmetric buckles. The composite layup definition for shell elements of both the surfaces was modeled with the following data provided as input for section properties: 1) shell thickness; 2) applicable material models, i.e., a) bi-linear isotropic strain hardening for the metallic shell as given in Table 3.2, and b) linear elastic orthotropic model for FRP as provided in Table 4.4 and case-specific properties given in Table 4.5; 3) orientation of element coordinate system; and 4) the number of integration points. Both surfaces were defined as the middle surface in the surface offset definition of the composite layup. The FRP thickness of 0.17 mm/0.05 mm was modeled as one layer in the composite layup definition of the FRP shell surface with five integration points through the thickness of the layer. Nine integration points were employed through the thickness of the shell elements representing the metallic shell surface. The modes and characteristics of the elastically and plastically buckled shells are pretty different from one another, and accordingly, applicable FRP strengthening methods should differ fundamentally.

Material property	Value
Elastic modulus along the radial direction, E_3 (GPa)	9.5
Poisson's ratio, $\nu_{12} = \nu_{13}$	0.27
Poisson's ratio, ν_{23}	0.4
Shear modulus, $G_{12} = G_{13}$ (GPa)	5.5
Shear modulus, G_{23} (GPa)	3.9

Table 4.4: General material properties of FRP wrap

Description	Shell nomenclature	Modulus of FRP wrap		Effective modulus of shell	
		E_h (GPa)	E_l (GPa)	E_{he} (GPa)	E_{le} (GPa)
Bare A1 shell	A1-F0	-	-	71	71
Varying longitudinal modulus of FRP wrap for A1 metallic shell (Case - 1A)	A1-F1-71GPa-71GPa	71	71	71	71
	A1-F1-65GPa-133GPa	65	133	71	80
	A1-F1-57GPa-271GPa	57	271	71	100
	A1-F1-52GPa-408GPa	52	408	71	120
	A1-F1-40GPa-958GPa	40	958	71	200
Varying circumferential modulus of FRP wrap for A1 metallic shell (Case - 1B)	A1-F1-5GPa-38GPa	5	38	62	71
	A1-F1-25GPa-66GPa	25	66	64	71
	A1-F1-50GPa-70GPa	50	70	68	71
	A1-F1-71GPa-71GPa	71	71	71	71
	A1-F1-100GPa-71GPa	100	71	75	71
	A1-F1-133GPa-65GPa	133	65	80	71
	A1-F1-209GPa-63GPa	209	63	91	71
	A1-F1-271GPa-57GPa	271	57	100	71
	A1-F1-340GPa-55GPa	340	55	110	71
	A1-F1-408GPa-52GPa	408	52	120	71
	A1-F1-958GPa-40GPa	958	40	200	71
Bare A2 shell	A2-F0	-	-	71	71

Table 4.5: Shell types and cases of FRP strengthening studied

Description	Shell Nomenclature	Modulus of FRP wrap		Effective modulus of shell	
		E_h (GPa)	E_l (GPa)	E_{he} (GPa)	E_{le} (GPa)
Varying circumferential modulus of FRP wrap for A2 metallic shell (Case - 2B)	A2-F1-71GPa-71GPa	71	71	71	71
	A2-F1-186GPa-63GPa	186	63	80	71
	A2-F1-313GPa-53GPa	313	53	90	71
	A2-F1-951GPa-22GPa	951	22	140	71
Bare A3 shell	A3-F0	-	-	71	71
Varying longitudinal modulus of FRP wrap for A3 metallic shell (Case - 3A)	A3-F1-71GPa-71GPa	71	71	71	71
	A3-F1-58GPa-239GPa	58	239	71	80
	A3-F1-41GPa-425GPa	41	425	71	90
	A3-F1-9GPa-985GPa	9	985	71	120
Varying circumferential modulus of FRP wrap for A3 metallic shell (Case - 3B)	A3-F1-9GPa-50GPa	9	50	68	71
	A3-F1-41GPa-70GPa	41	70	69	71
	A3-F1-58GPa-71GPa	58	71	70	71
	A3-F1-71GPa-71GPa	71	71	71	71
	A3-F1-239GPa-58GPa	239	58	80	71
	A3-F1-425GPa-41GPa	425	41	90	71
Bare A4 shell	A4-F0	-	-	71	71
Varying longitudinal modulus of FRP wrap for A4 metallic shell (Case - 4A)	A4-F1-71GPa-71GPa	71	71	71	71
	A4-F1-69GPa-110GPa	69	110	71	85
	A4-F1-68GPa-151GPa	68	151	71	100
	A4-F1-66GPa-207GPa	66	207	71	120
	A4-F1-63GPa-400GPa	63	400	71	190
Varying circumferential modulus of FRP wrap for A4 metallic shell (Case - 4B)	A4-F1-35GPa-70GPa	35	70	58	71
	A4-F1-71GPa-71GPa	71	71	71	71
	A4-F1-110GPa-70GPa	110	70	85	71
	A4-F1-151GPa-68GPa	151	68	100	71
	A4-F1-207GPa-66GPa	207	66	120	71
	A4-F1-400GPa-64GPa	400	64	190	71
Varying longitudinal modulus of FRP wrap for A4 metallic shell (Case - 4A')	A4-F1'-71GPa-71GPa	71	71	71	71
	A4-F1'-68GPa-151GPa	68	151	71	82
	A4-F1'-63GPa-400GPa	63	400	71	118
Varying circumferential modulus of FRP wrap for A4 metallic shell (Case - 4B')	A4-F1'-71GPa-71GPa	71	71	71	71
	A4-F1'-151GPa-68GPa	151	68	182	71
	A4-F1'-400GPa-63GPa	400	63	118	71

Bare A5	A5-F0	-	-	71	71
Varying longitudinal modulus of FRP wrap for A5 metallic shell (Case - 5A)	A5-F1-71GPa-71GPa	71	71	71	71
	A5-F1-58GPa-250GPa	58	250	71	75
	A5-F1-30GPa-480GPa	30	480	71	80
	A5-F1-5GPa-930GPa	5	930	71	90
Description	Shell Nomenclature	Modulus of FRP wrap		Effective modulus of shell	
		E_h (GPa)	E_l (GPa)	E_{he} (GPa)	E_{le} (GPa)
Varying circumferential modulus of FRP wrap for A5 metallic shell (Case - 5B)	A5-F1-25GPa-69GPa	25	69	70	71
	A5-F1-71GPa-71GPa	71	71	71	71
	A5-F1-250GPa-58GPa	250	58	75	71
	A5-F1-480GPa-30GPa	480	30	80	71
	A5-F1-930GPa-5GPa	930	5	90	71

Table 4.6: Shell types and cases of FRP strengthening studied

The imperfections in the metallic shell surface due to fabrication tolerances lower the buckling capacity of shells. This imperfection sensitivity is more for shells buckling elastically and relatively less for shells buckling plastically [74]. Although the present study was focused on bringing out the qualitative effects of FRP strengthening, a very small geometric imperfection [16] of the form given by Eq. (4.4) was employed. This imperfection will only act as a trigger for initiating the buckling. This form was a combination of an axisymmetric and asymmetric buckling, i.e., continuous symmetric buckles in sine form in the longitudinal direction and two lobes in the circumferential direction corresponding to the shape of the shell from the first mode of the Eigenvalue analysis. The radial offset \square of imperfection in a perfect cylindrical shell surface is given by in which an imperfection amplitude of 0.01 mm was employed based on the parametric study to match with experimental results of Teng and Hu [16], is along the longitudinal direction, provides two lobes in the circumferential direction, and is the critical half-wavelength for the classical axisymmetric elastic buckling mode of axially compressed cylinders and is equal to 1.728. The imperfection form given by Eq. (4.4) was calculated for all five cases of shells employed in the numerical study.

4.3 EXPERIMENT VALIDATION

The experimental work of Teng and Hu [16] was numerically simulated to validate the FEA methodology adopted in the present study. A detailed validation of this FEA approach with experimental work [16] is available in the previous study [77] and is briefly mentioned here. Different cases of GFRP strengthening with 0, 1, and 2 layers of unidirectional wrap in circumferential direction were numerically simulated employing the methodology discussed in Sec-3.4.1. Steel shell and FRP wrap were modeled as two separate shell surfaces accounting for all the orthotropic properties of FRP wrap, initial imperfections in shell surface, and explicit modeling of FRP overlap. Different cases of analyses with all the combinations of damage models, viz. metal-FRP interfacial damage model, and intralaminar FRP damage model, were analysed. It is brought out that even without the inclusion of interfacial bond behaviour, the point of strain localization could be accurately predicted. With the exclusion of interfacial damage, the comparison of numerical analyses with experimental results is shown in Figure 4.3. This attempt validates the presently

adopted FEA methodology in predicting the buckling behaviour of different shell types with different cases of FRP strengthening studied in this paper. In Figure 3.3, the ST-indicates steel tube, F-indicates FRP wrap, and the number following F-indicates the number of FRP wrap plies.

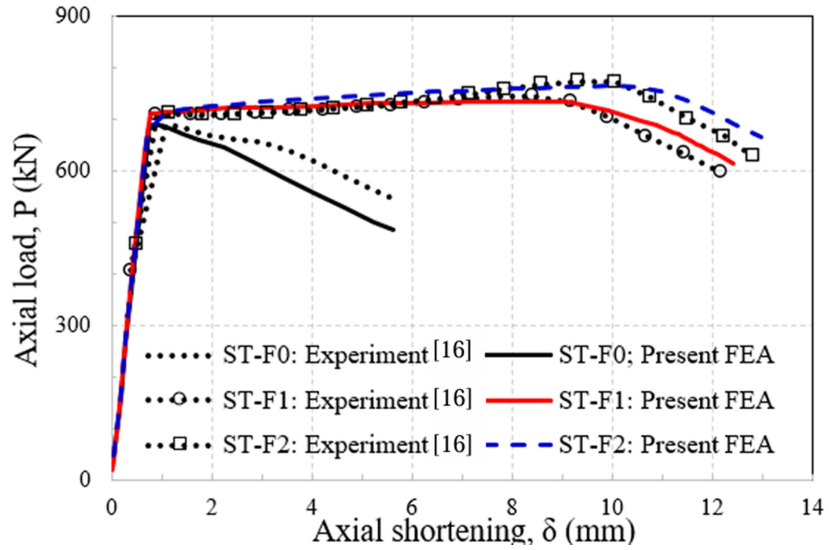


Figure 4.3: FEA simulations and experimental results [77]

4.4 Effect of FRP Strengthening on buckling behavior

The buckling characteristics of the five bare metallic shell types identified in Sec 3.2 and the effects of FRP strengthening for each shell type were investigated in this section. General behavior of FRP strengthened shells Before discussing the numerical results, to explore the effect of FRP strengthening on metallic cylindrical shells, the general buckling behavior of the FRP strengthened shells exhibiting different stages of buckling, as shown in Figure 4.4, is brought out and discussed in order to have a clear understanding. Though it is a generic 66 case of plastically buckling FRP strengthened shell, it encompasses all variations in the buckling behavior of the FRP strengthened shells, including the elastic buckling. Plastic buckling shells are the ones that yield before buckling. Pre-yield stiffness of the shell will be equal to the effective modulus of the strengthened shells along the longitudinal direction . The first yielding always happens in the local bending region near ends because of end restraints to shell wall displacements and rotations. The yielding of metallic shells in the local bending region will always lead to the formation of the axisymmetric buckle. The point of yielding YP is marked as YP/B1

in Figure 4.4, representing the point of axisymmetric buckling initiation B1. The point of loading until YP/B1 is termed Stage-1.

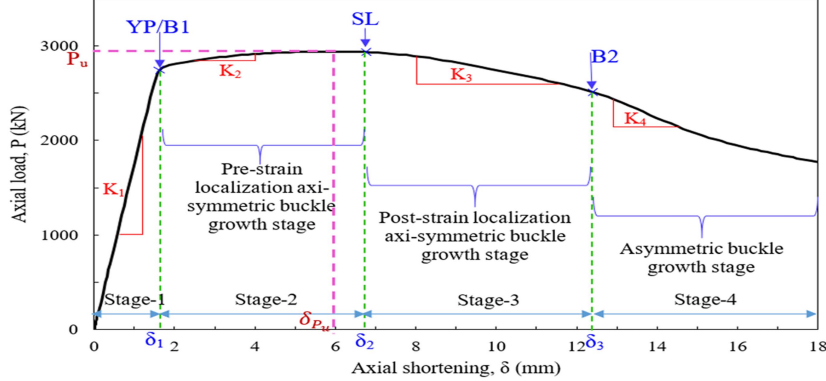


Figure 4.4: Different stages of buckling

The imperfections in the metallic shell surface due to fabrication tolerances lower the buckling capacity of shells. This imperfection sensitivity is more for shells buckling elastically and relatively less for shells buckling plastically [74]. Although the present study was focused on bringing out the qualitative effects of FRP strengthening, a very small geometric imperfection [16] of the form given by Eq. (4.4) was employed. The FE modeling and analysis were carried out in ABAQUS [61]. The FE model similar to Krishna et al. [77] was also employed in this study, briefly described here. The metallic cylindrical shell and the FRP wrap were modeled as two separate shell surfaces of the same diameter viz. $\emptyset 300$ mm. The tie constraint was introduced between the metallic shell's outer surface and the FRP wrap's inner surface. Both the surfaces were discretized with quadrilateral shell elements (S4R), which linearly interpolate the field variable and capture the finite-membrane strain with reduced integration. These elements were more robust without leading to convergence difficulties, even in the presence of steep deformation gradients around the axisymmetric bulge region and asymmetric buckles

Yielding of the shell will lead to a sudden drop in modulus of the metallic portion of the shell to a very low value, which is close to 1/100th of its elastic modulus. However, because of the presence of FRP wrap, the post-yield effective modulus of FRP strengthened shell K2 will be relatively high compared to that of the bare shell. Further loading would lead to the growth of the axisymmetric buckle and the global outward bulging of the shell wall. The growth of the axisymmetric buckle would lead to the eccentricity of loads acting through the shell wall from the pivot point of

bending, i.e., the axisymmetric peak. As the axisymmetric buckle grows, the eccentricity of load increases, increasing bending moment acting at the axisymmetric fold, thereby 67 increasing the total axial displacement. After a particular stage of growth of the axisymmetric buckle, the contribution to the axial displacement will be totally from the outward bulging happening at the axisymmetric buckle region. This point in the buckling behavior is termed here as strain localization, marked as SL in Figure 3.4. So the pre-strain localization stiffness K2 decreases and would be near zero at the point of strain localization. Relatively large bending moments act in axisymmetric folds compared to the rest of the shell wall where global outward bulging is happening. So larger amount of eccentricity in loading at folds nullifies the effect of resistance offered by FRP wrap. This phenomenon will lead to a steeper stiffness drop when axial shortening is completely due to outward bulging at the axisymmetric buckle region. The region of buckling between YP and SL is termed Stage-2 in Figure 3.4. This stage in strengthened shells would involve a positive slope and a slight increase in load until the point of SL, unlike the case of the bare metallic shells. In bare metallic shells, the post-yield modulus K2 is very low, leading to relatively faster growth of the axisymmetric buckle to the point of SL. In thin bare shells, the flexural resistance of the shell to local bending is also less, so strain localization immediately follows the initiation of axisymmetric growth, leading to an immediate drop in load, post yielding. Relatively thicker FRP strengthened shells with a higher amount of strengthening exhibit a clear and considerably large Stage-2. Further loading beyond SL would lead to a drop in load. Stiffness K3 gradually decreases with growth in axisymmetric buckle even beyond SL because of the continuous increase in eccentricity. The asymmetric buckle appears after a particular stage of growth of the axisymmetric buckle around the axisymmetric buckle region marked as B2 in Figure 4.4. The post-strain localization axisymmetric buckle growth stage between SL and B2 is termed Stage-3. Beyond B2, the stiffness K4 drop was initially much steeper because of asymmetric buckle initiation. The asymmetric buckle growth stage will usually be much more stable and involves a lesser drop in load. The asymmetric buckle growth stage after B2 is termed as Stage-4 behavior. However, Stage-4 will be less important from the structural applications point of view as the load would have dropped to a less value. The most general plastic buckling behavior, which is brought out using Figure 4.4, undergoes wide variations with changes in ratio and change in the amount and type

(i.e. direction) of FRP strengthening. Details about different variations of this general buckling behavior in plastically buckling shells are brought out and explained in Sec 3.5.2. The typical behavior of the elastic buckling of FRP strengthened shells is given in 68 Sec-3.5.1, which was characterized by the absence of Stages-2 and 3 and the sudden appearance of asymmetric buckling. The axial shortening δ of the strengthened shell at various salient points are represented as δ_1 at point of YP/B1, δ_2 at the point of SL, δ_3 at point of asymmetric buckle initiation B2 and at ultimate buckling capacity P_u , in Figure 4.4. A1 shell The A1 metallic shell is an aluminum shell of 1 mm uniform thickness. The shell diameter is 300 mm and has a the ratio of 150. It possesses an elastic buckling capacity of 273 kN and a yield capacity of 358 kN, as mentioned in Table 4

.3. This is an elastically buckling shell since its elastic buckling capacity is lower than its yield capacity. The elastic buckling is a pure geometric instability. It does not give any indication prior to buckling and is characterized by the sudden appearance of buckles and rapid loss of load-carrying capability of the cylindrical shell. The elastic buckling modes are asymmetric, involving alternate inward and outward displacement of the shell wall and are spread over the full length of the shell. They appear in full size even at the first instance of buckling and subsequently do not grow appreciably. The size and spread of buckles result in a steep and a large drop in the load. Ensuing sudden loss of load capacity is steep, dropping load capacity to < 30% of the value at the instance of buckling (i.e., P_u).

4.5 FINAL BUCKLING PERFORMANCE

The buckling performance of metallic shells can be enhanced by external wrapping with a thin layer(s) of FRP composite. This paper highlighted the importance of considering the buckling characteristics and buckling modes of the bare metallic shell to arrive at effective methods and the amount of FRP strengthening. Initially, the most general buckling behavior of FRP strengthened metallic shells exhibiting clear yield point, point of strain localization around axisymmetric buckling location, and asymmetric buckle initiation point was brought out. Wide variations in the general buckling behavior under the influence of different parameters of FRP strengthened shell vibration (ranging from 20 to 500), yield strength of metallic shell material, and elastic modulus, direction, and amount of FRP strengthening were

studied.

The following conclusions and recommendations can be drawn from the research work:

The elastic modulus of FRP strengthened metallic shell

- 1) will always be equal to the of strengthened shell irrespective of the type of shell and strengthening, and
- 2) will increase only by employing FRP with higher than E of the metallic shell.

For the elastically buckling shells with $t > 5$ times the FRP wrap thickness, the P_u can be increased only by increasing the h of the FRP wrap. An increase if the FRP wrap causes no change in the buckling load capacity of shells.

For elastically buckling shells with $t < 2$ times the FRP wrap thickness, the FRP strengthening increases the P_u even with an increase in of the FRP.

For the metallic shells buckling plastically, the greater the difference between the elastic buckling load capacity and the yield capacity, the greater the possible .

Plastically buckling bare shells with >30 undergo asymmetric buckling beyond a certain stage of growth of axisymmetric buckle post yielding. For shells of this type:. So a relatively smaller increase in P_u was realized. A large increase in ductility was achieved even with a small increase in h of the FRP. Beyond a certain amount of increase in the ductility decreases with stiffening. While ductility always increases with an increase in h .

Therefore, circumferential stiffening was more beneficial in increasing the ductility of these shells. the axisymmetric peak. As the axisymmetric buckle grows, the eccentricity of load increases, increasing bending moment acting at the axisymmetric fold, thereby 67 increasing the total axial displacement. After a particular stage of growth of the axisymmetric buckle, the contribution to the axial displacement will be totally from the outward bulging happening at the axisymmetric buckle region. This point in the buckling behavior is termed here as strain localization, marked as SL in Figure 3.4. So the pre-strain localization stiffness K2 decreases and would be near zero at the point of strain localization.

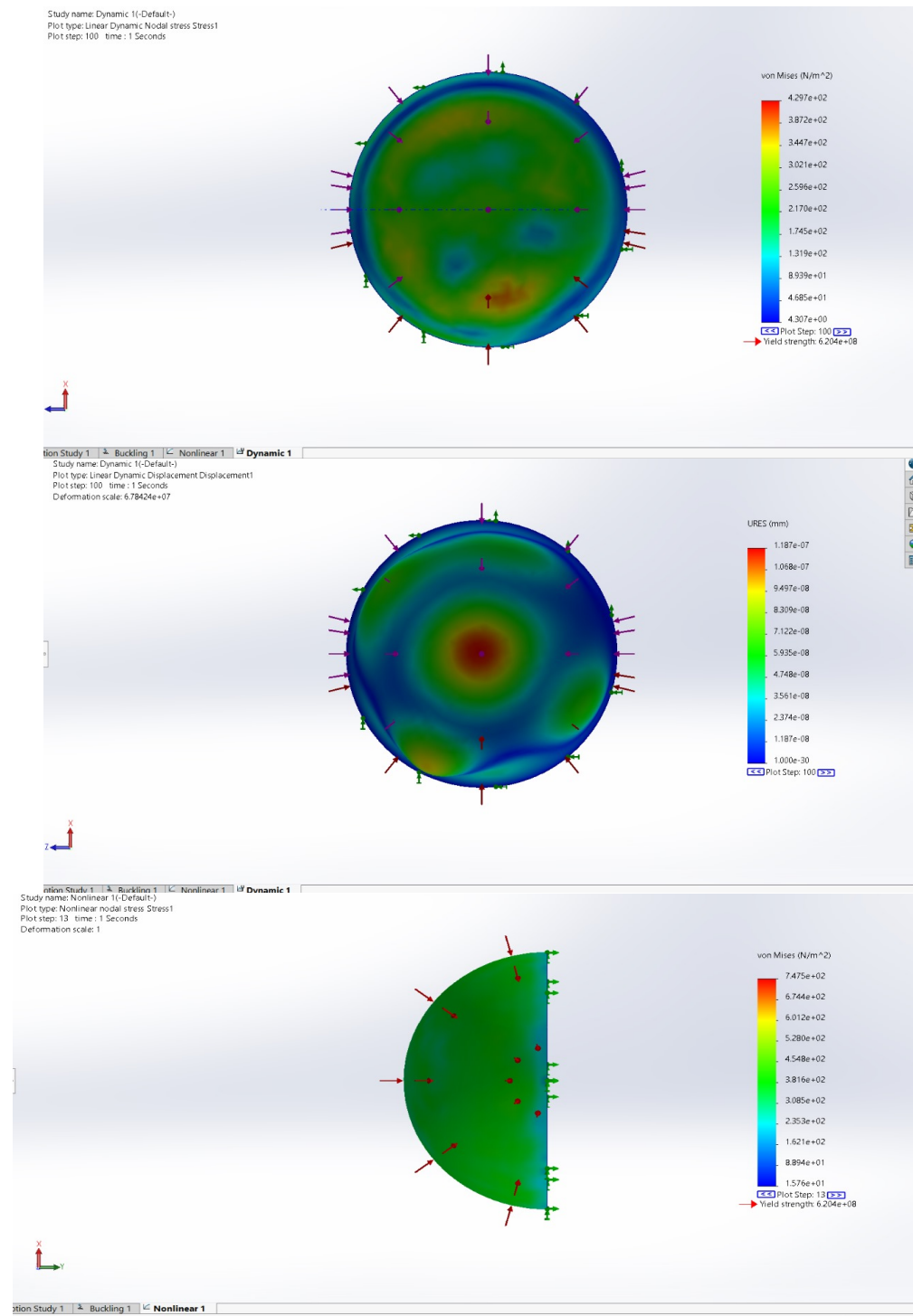


Figure 4.5: buckling analysis with 3mm thickness of steel.

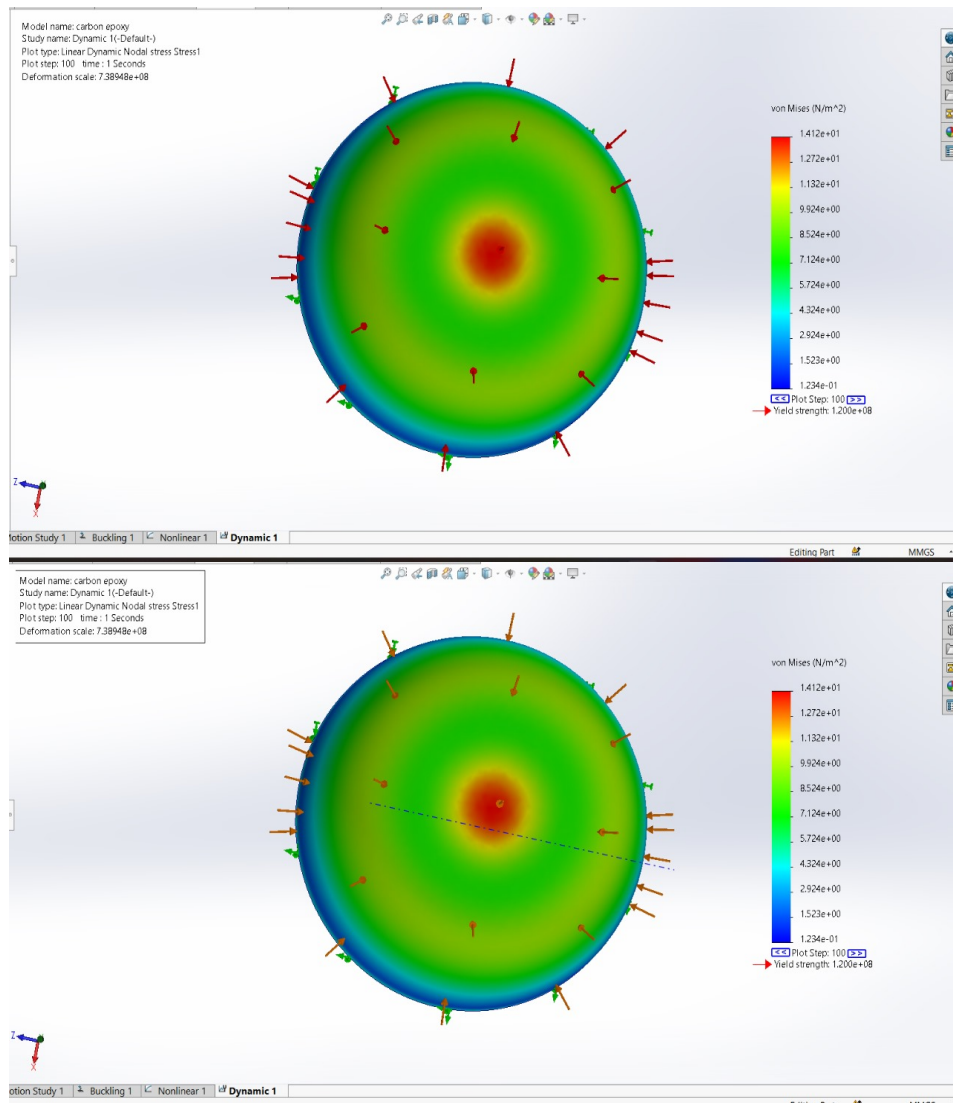


Figure 4.6: Buckling analysis with 2.5mm thickness of steel and composite mix with carbon epoxy.

The fig 4.5 and 4.6 shows the buckling analysis of steel and fibre reinforced polymer of carbon epoxy mix so that the stability of the missile increases, when a ballistic missile is launched into the water it travels with low speed compared to of air as water acts more pressure on it opposing the speed of missile in opposite direction.so, as to increase the efficiency of the missile the composite layer is added. The effective modulus of the FRP strengthened metallic shell along the longitudinal and transverse directions were calculated from the concepts of classic lamination theory where direction 1 is defined along the longitudinal direction.

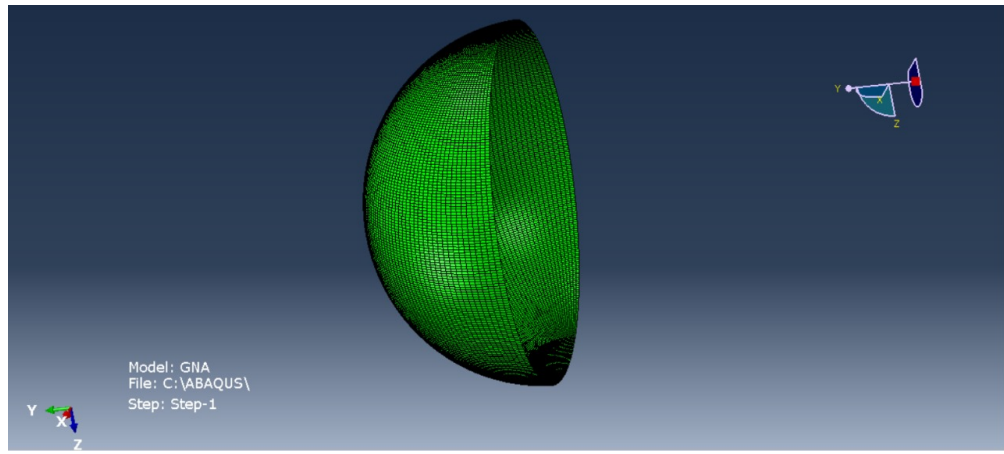


Figure 4.7: Meshing of steel

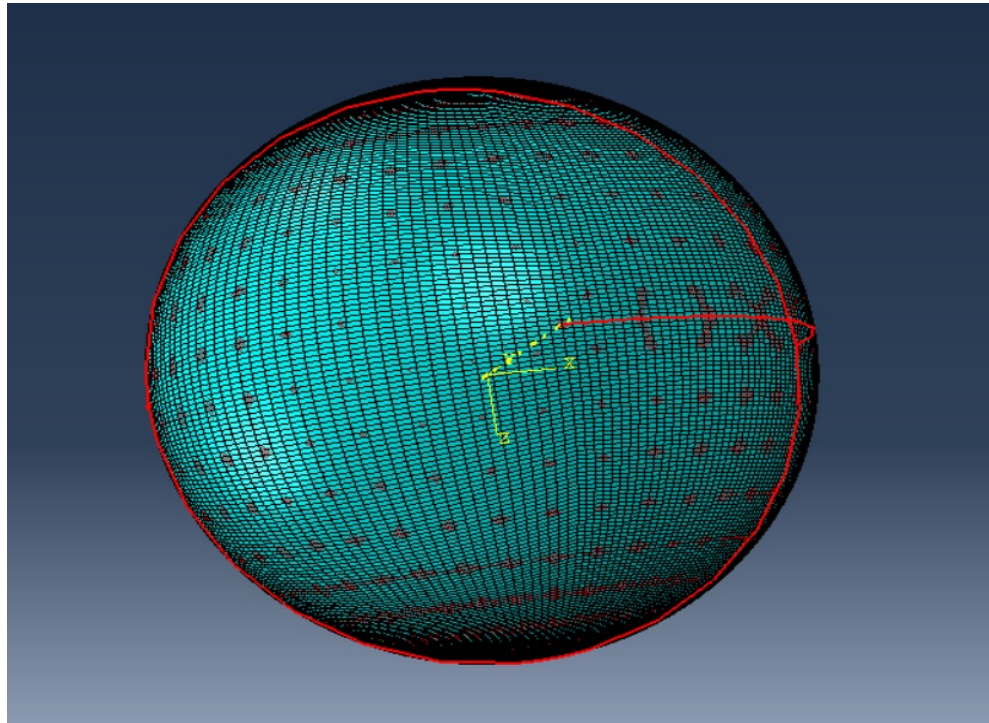


Figure 4.8: Meshing of Carbon Epoxy layer.

At the beginning we added carbon epoxy layer on the steel layer but the attaching or mating is not done to perfection so as to mate them to perfection we separately mated them using ABAQUS software. The fig 4.7 & 4.8 shows the individual meshing of both the materials this enhances the efficiency of the FRP shell.

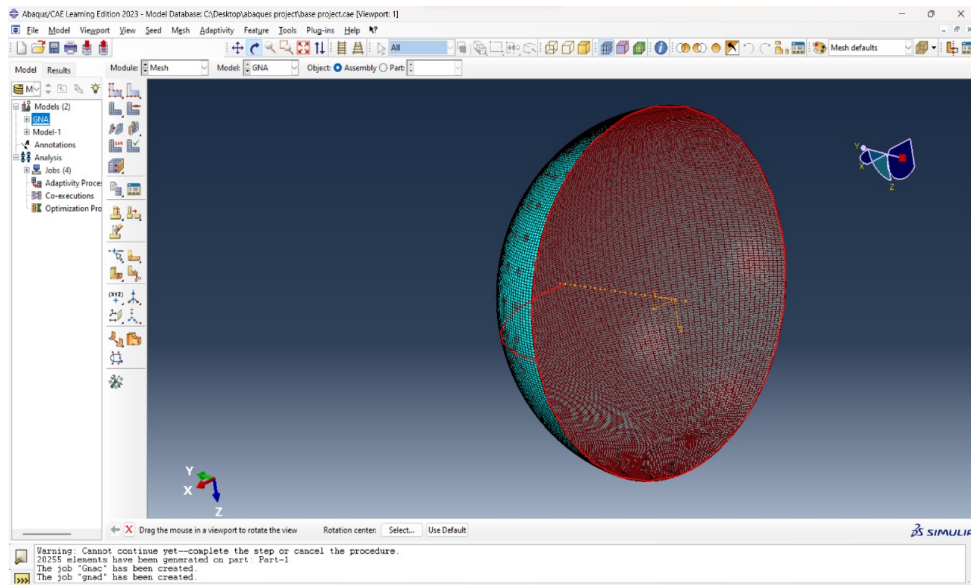


Figure 4.9: Combined mesh.

The fig 4.9 shows the combination mesh of the corresponding two individual components that is steel (15CdV6) and carbon epoxy.

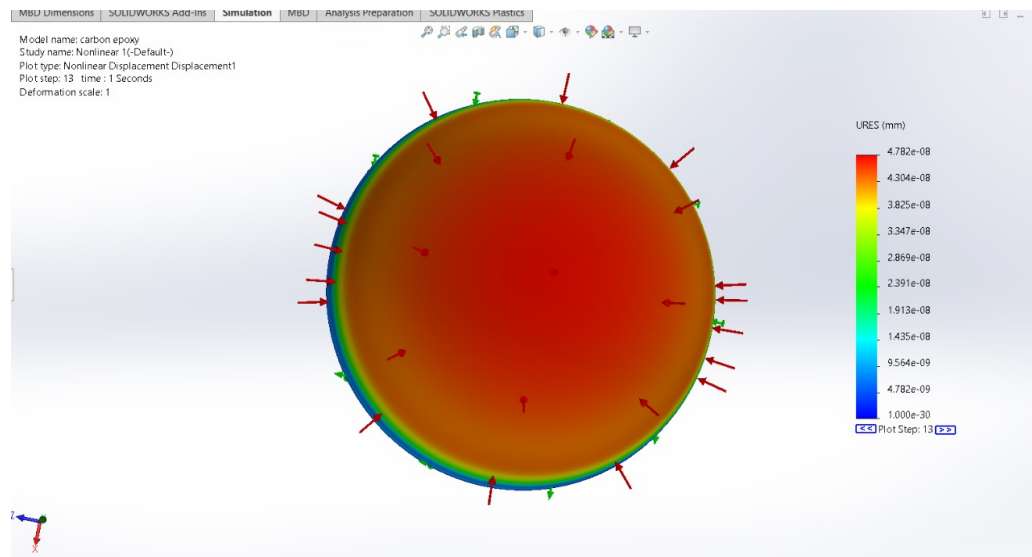


Figure 4.10: The buckling analysis with 2mm composite thickness and 1mm steel.

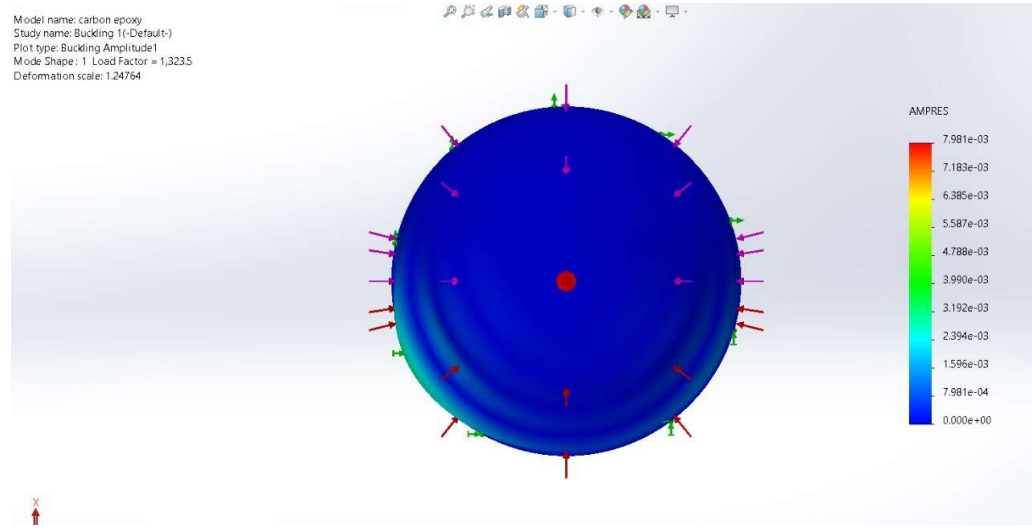


Figure 4.11: analysis done with 1.5mm steel and 1.5 mm thickness of composite.

SL. NO.	STEEL THICKNESS	CARBON THICKNESS	LOAD FACTOR	VALUE AT WHICH IT STARTS BUCKLING	DEFORMATION SCALE
1.	3mm	0mm	6.5135e+07	6.513	0.00902493
2.	0mm	3mm	2.8082e+07	2.808	0.00981807
3.	1.5mm	1.5mm	9.1374e+07	9.137	0.00801024
4.	1mm	2mm	1.29874e+07	1.298	0.00933465
5.	0.5mm	2.5mm	0.23952e+07	0.239	0.00733133
6.	2.5mm	0.5mm	5.1674e+07	5.1674	0.00971711

Table 4.7: The results table of variety of thicknesses and their corresponding load factors.

The figures 4.10 and 4.11 shows the variety of thicknesses and it is clearly observed that the strength of the buckling and durability is maximum with 1.5 mm thickness of 15CdV6 steel and 1.5mm thickness of carbon epoxy layer this can be modified and enhanced with some other materials.

Chapter-5

Live Testing And Examination

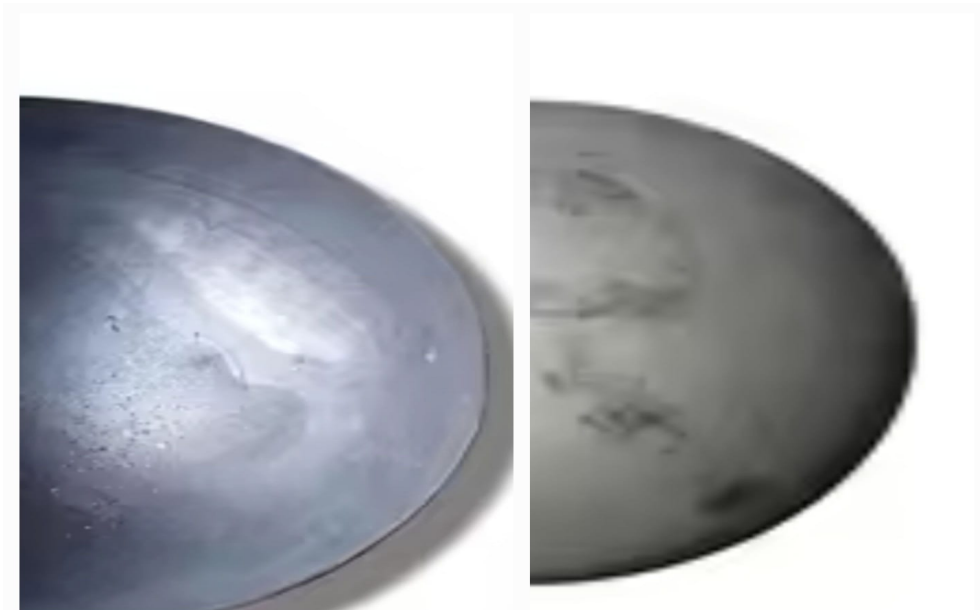


Figure 5.1 : Hemisphere with carbon epoxy on one side and steel on the other side.

As shown in fig 5.1 the steel is cut to 1.5mm thickness and a 1.5mm thickness is coated on it and then the required model is made and then sent it for the testing. In general the steel and composite should made dry and let the model gets hard and then the testing is done with suitable equipment. Depending upon the force and pressure applied under water then the buckling is done the values are being calculated and the results are obtained. There is a special apparatus designed for the buckling of cylindrical, spherical and hemispherical models. For cylindrical models the pressure is applied on the circumference of the two circular ends and for spherical and hemispherical models the pressure is applied on different locations of the body and the suitable part. In structural engineering, buckling is an important occurrence, especially in steel constructions. It is critical to comprehend buckling behavior and the mitigating techniques that can be used to maintain structural integrity and safety. The goal of this study is to improve the performance of steel structures with composite layer mixes by examining their buckling behavior under varied loading scenarios. When a structural member gives way under compressive loads because of instability, it is said to have buckled. If left unchecked, steel constructions are prone

to buckling, particularly in thin members, which can result in catastrophic failures. Composite layer mixes have demonstrated potential in improving structural resilience and reducing buckling hazards by combining steel with other materials such as concrete or fiber-reinforced plastics.



Figure 5.2: Buckle testing apparatus for cylinders.

In engineering and material science research, a hemisphere's buckling testing apparatus is essential. Examining the structural stability, deformation, and failure modes of hemispherical structures under compressive loads is made easier with its assistance. This paper explores the purpose, construction, and importance of buckling testing equipment for hemispherical structural behavior. As shown in Fig 5.2 Hemisphere buckling testing equipment usually includes of a robust foundation, a loading mechanism, support fixtures, and data collecting instrumentation. The entire setup is supported and stabilized by the base. Buckling is caused by compressive loads that are applied to the hemisphere by the loading mechanism. During testing, support fixtures firmly keep the hemisphere in position, guaranteeing consistent loading and precise results. Furthermore, data collecting systems and sensors are integrated to quantify variables like deformation, load, and displacement. The hemisphere is subjected to controlled compressive loads until buckling occurs, which

is the main purpose of the buckling testing device. Through this procedure, scientists can examine the structure's buckling behavior, critical load, and mechanism of collapse. They can examine the stability of the hemisphere in various scenarios and track the patterns of deformation by gradually increasing the load. The device allows for exact control over the parameters of the test, guaranteeing the repeatability and dependability of the outcomes. For many different engineering applications, it is crucial to comprehend the buckling behavior of hemispherical structures. For example, hemispherical shells are frequently utilized in spaceship components, domes, and pressure containers in aerospace engineering. Understanding their buckling properties is essential to building sturdy and secure structures. Similar to this, research on buckling phenomena in material science sheds light on the mechanical characteristics and structural integrity of various materials. Researchers can validate theoretical models, optimize designs, and create novel materials with better buckling resistance by employing the device to conduct buckling tests. A hemispheric buckling test apparatus is a fundamental tool in engineering and material sciences. It facilitates the analysis of structural stability, deformations, and failures of hemispheric structures under compression loads. This paper examines the purpose, design, and significance of hemispheric testing equipment for structural behavior.

Additionally, the buckling testing apparatus is a useful teaching tool for engineering professionals and students. It enables them to obtain practical knowledge in structural analysis, design optimization, and experimental mechanics. In structural engineering, buckling is an important occurrence, especially in steel constructions. It is critical to comprehend buckling behavior and the mitigating techniques that can be used to maintain structural integrity and safety. The goal of this study is to improve the performance of steel structures with composite layer mixes by examining their buckling behavior under varied loading scenarios. When a structural member gives way under compressive loads because of instability, it is said to have buckled. If left unchecked, steel constructions are prone to buckling, particularly in thin members, which can result in catastrophic failures. Composite layer mixes have demonstrated potential in improving structural resilience and reducing buckling hazards by combining steel with other materials such as concrete or fiber-reinforced plastics.

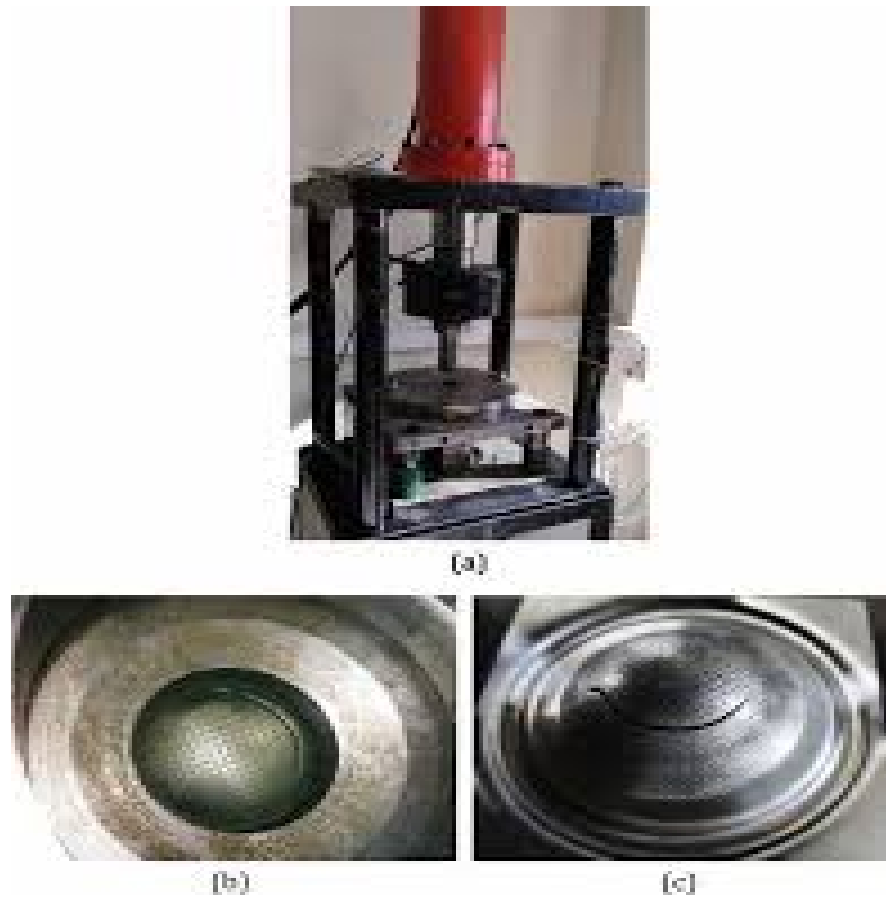


Figure 5.3: Buckle testing apparatus for hemisphere and (b), (c) shows after buckling.

To sum up, the hemisphere buckling testing device is an essential instrument for material science and engineering research. This apparatus allows researchers to investigate the finer points of structural stability, deformation, and failure processes in hemispherical structures with great care and precision in its design and operation. Through the application of controlled compressive loads to these structures, researchers can gain important understandings of their failure mechanisms.

The significance of these devices spans numerous engineering fields, including civil and aerospace engineering, where hemispherical structures are utilized in spaceship components, pressure tanks, and domes. It is crucial to comprehend the buckling properties of these structures while building secure systems that will function well under a range of operating circumstances.

In addition, it is a great educational tool for students and professionals. Through practical experimentation, students and professionals can gain a better understanding

of the principles of engineering. They can also gain insight into the real-world problems related to structural stability and failures. We are constantly pushing innovation and design boundaries in engineering. Buckling testing apparatus validates theoretical models, optimizes designs, and develops advanced materials with improved buckling resistance capabilities. Its role in research as well as in education highlights its importance in shaping tomorrow's engineering and technology landscape. Essentially, the Buckle Test Automation for Hemispheres is a symbol of human creativity and scientific curiosity. It allows us to unlock the secrets of structural behavior, paving the way to safer and more resilient structures for years to come. At its core, the hemispheric buckling testing apparatus is a testament to human creativity and science, allowing us to unlock the secrets of structural behavior and advance the development of safer, stronger structures for decades to come.

Chapter-6

Summary and Conclusion

6.1 SUMMARY

The FRP strengthening of metallic shell structures is brought out as an attractive retro-fit strengthening technique to significantly improve the buckling capacity and ductility of metallic shell structures. A few research gaps were identified in this field of metal-FRP hybrid shell structures, and the thesis research is aimed to address them as elaborated below.

- An accurate numerical prediction method is developed for carrying out buckling analysis of metal-FRP hybrid shells accounting for different aspects specific to metal-FRP hybrid shells viz. locating shell element's reference surface through the thickness of the shell, FRP overlap modelling as well accounting for interfacial damage and intra laminar FRP damage.
- The effect of interfacial and intra laminar damage on the buckling behavior of hybrid shell structures is brought out.
- The effectiveness of FRP strengthening methods on buckling behavior of shells of all possible r/t ratios, encompassing elastic, transitional, and plastic buckling modes, is demonstrated.
- The generalized buckling behavior of metal-FRP hybrid shell structures is brought out.
- Effective FRP strengthening methods for metallic shells exhibiting elastic or transitional or plastic buckling modes are proposed.
- Imperfection sensitivity of hybrid shell structures of all possible r/t ratios is brought out.
- Variation in imperfection sensitivity with the amount of circumferential directional FRP strengthening for all possible r/t ratios is brought out.

6.2 CONCLUSION

The significant conclusions that can be drawn from the present thesis on metal-FRP hybrid shell structures are summarized below.

- Interfacial and intralaminar FRP damage phenomena only affect post-yield behaviour.
- These damage models are required to accurately predict strain localization points and buckling modes of plastically buckling shells.
- FRP circumferential strengthening is effective for elastically buckling shells in increasing their buckling capacity as well as ductility.
- Longitudinal FRP strengthening is effective for plastically buckling shells in increasing their buckling load capacity.
- Imperfection sensitivity of transitionally buckling shells reduces with the optimal amount of FRP strengthening.
- FRP wrapping resists lip opening, alleviates stress concentration effects, and suppresses weak buckling modes for shells with cut-outs, thereby significantly increasing the buckling capacity for different cut-out configurations of hybrid shell structures.

6.3 FUTURE SCOPE

The future works can include the following areas:

- Establishing design equations for FRP strengthened metallic shell structures for predicting buckling capacity and ductility of hybrid shell structures accounting for shell's r/t ratio, shell diameter, FRP properties, FRP orientation, and number of wraps for hybrid shells of all possible r/t ratios.
- Experimental validation of buckling behavior of elastically buckling aero-space shell structures featured with cutouts
- Thermal softening of wrapped FRP is to be modeled to predict the buckling behaviour of aerospace hybrid shell structures during flight kinetic heating.
- Vibration attenuation characteristics of hybrid shell structures and hybrid shell structures for combined loading scenarios can be explored.

REFERENCES

- [1] C.T. Sun, W. Qian. The use of finite extension strain energy release rates in fracture of interfacial cracks, International Journal of Solids and Structures Volume 34, Issue 20, Pages 2595-2609, July 1997
- [2] Nilima Roy, Arpan Das, Ashok Kumar Ray, Structural Integrity and Uncertainty in Creep Damage Assessment of Service Exposed Reformer Tubes, Procedia Engineering, Volume 86, pp. 858-869, 2014.
- [3] R. Ganesan, A Stochastic Modeling and Analysis Methodology for Quantification of Fatigue Damage, Compute. Methods Appl. Mech. Eng., 190, pp. 1005-1019, (2000).
- [4] N. Roy, S.C. Bose, R.N. Ghosh, Stochastic aspects of evolution of creep damage in austenitic stainless steel, Mat. Sc. Engg. A, 527, pp. 4810-4817, (2010).
- [5] N. P.O'Dowd, C. F. Shih, and M. G. Stout, "Test geometries for measuring interfacial fracture toughness," International Journal of Solids and Structures, vol. 29, pp. 571-589, 1992.
- [6] B. D. Davidson and V. Sundararaman, "A single leg bending test for interfacial fracture toughness determination," International Journal of Fracture, vol. 78, pp. 193-210, 1996.
- [7] Hongqin Yang, An interaction crack growth model for creep-brittle superalloys with high temperature dwell time. Engineering Fracture Mechanics, Volumes 124–125, pp. 112-120, 2014.
- [8] J. R. Rice, "A path independent integral and the approximate analysis of strain concentration by notches and cracks," Journal of applied mechanics, vol. 35, pp. 379- 386, 1968.
- [9] E.F. Rybicki et al, A finite element method calculation of stress intensity factors by a modified crack closure integral Eng. Fract. Mech. (1977).
- [10] Lanqing Tang, Caifu Qian, Experimental study of the strain-strengthening effect on the mixed mode notch-crack fatigue propagation in austenitic stainless steel 06Cr19Ni10. Engineering Fracture Mechanics, Volume 134, pp. 54-60, 2015.
- [11] Carla Beckmann, Effects of material uncertainty in the structural response of metal foam core sandwich beams, Composite Structures, Volume 113, pp. 382-395, 2014.

- [12] Jialai Wang and Chao Zhang, Nonlinear fracture mechanics of flexural shear crack induced debonding of FRP strengthened concrete beams, International Journal of Solids and Structures, Volume 45, pages 2916–2936, 2008.
- [13] Shaat A, Fam A. Axial loading tests on short and long hollow structural steel columns retrofitted using carbon fibre reinforced polymers. Canadian Journal of Civil Engineering 2006; 33(4): 458–470. DOI: 10.1139/l05-042.
- [14] Harries KA, Peck AJ, Abraham EJ. Enhancing stability of structural steel sections using FRP. Thin-Walled Structures 2009; 47(10): 1092–1101. DOI: 10.1016/j.tws.2008.10.007.
- [15] . Teng JG, Rotter JM. Buckling of thin shells - An overview. In: Teng JG, Rotter JM, editors. Buckling of thin metal shells, London; New York: Spon Press; 2004.
- [16] Pircher M, Bridge R. Buckling of Thin-Walled Silos and Tanks under Axial Load— Some New Aspects. Journal of Structural Engineering-Asce - J STRUCT ENG-ASCE 2001; 127. DOI: 10.1061/(ASCE)0733-9445(2001)127:10(1129).
- [17] Pircher M, Bridge R. Buckling of Thin-Walled Silos and Tanks under Axial Load— Some New Aspects. Journal of Structural Engineering-Asce - J STRUCT ENG-ASCE 2001; 127. DOI: 10.1061/(ASCE)0733-9445(2001)127:10(1129).
- [18] Fawzia S, Zhao XL, Al-Mahaidi R. Bond-slip models for double strap joints strengthened by CFRP. Composite Structures 2010; 92(9): 2137–2145. DOI: 10.1016/j.compstruct.2009.09.042.
- [19] Nguyen TC, Bai Y, Zhao XL, Al-Mahaidi R. Mechanical characterization of steel/CFRP double strap joints at elevated temperatures. Composite Structures 2011; 93(6): 1604–1612. DOI: 10.1016/j.compstruct.2011.01.010.
- [20] Liu HB, Zhao XL, Al-Mahaidi R. Effect of fatigue loading on bond strength between CFRP sheets and steel plates. International Journal of Structural Stability and Dynamics 2010; 10(01): 1–20. DOI: 10.1142/S0219455410003348.
- [21] Soroush M, Fard KM, Shahravi M, Soroush M, Fard KM, Shahravi M. Finite Element Simulation of Interlaminar and Intralaminar Damage in Laminated Composite Plates Subjected to Impact. Latin American Journal of Solids and Structures 2018; 15(6). DOI: 10.1590/1679-78254609.

